metals

MDPI

Article

Recrystallization and Grain Growth of AISI 904L Super-Austenitic Stainless Steel: A Multivariate Regression Approach

Giulia Stornelli [1,*], Matteo Gaggiotti [2], Silvia Mancini [2], Giuseppe Napoli [3], Claudia Rocchi [3], Chiara Tirasso [3] and Andrea Di Schino [2]

[1] Dipartimento di Ingegneria Industriale, Università Degli Studi di Roma "Tor Vergata", Via del Politecnico 1, 00133 Rome, Italy
[2] Dipartimento di Ingegneria, Università Degli Studi di Perugia, Via G. Duranti 93, 06125 Perugia, Italy; matteo.gaggiotti@studenti.unipg.it (M.G.); silvia.mancini@studenti.unipg.it (S.M.); andrea.dischino@unipg.it (A.D.S.)
[3] Acciai Speciali Terni S.p.A., Viale B. Brin, 05100 Terni, Italy; giuseppe.napoli@acciaiterni.it (G.N.); claudia.rocchi@acciaiterni.it (C.R.); chiara.tirasso@acciaiterni.it (C.T.)
* Correspondence: giulia.stornelli@students.uniroma2.eu

Abstract: AISI 904L is a super-austenitic stainless steel that is remarkable for its mechanical properties and high corrosion resistance, which strictly depend on its chemical composition and microstructural features. The recrystallization process and grain growth phenomena play key roles in achieving high levels of material quality, as often requested by customers for specific applications. In this paper, the evolution of the microstructure and hardness values after cold rolling and subsequent annealing is reported, with the aim of optimizing the thermomechanical treatment conditions and improving the efficiency of the production process. The investigation was focused on three different cold reduction ratios (50%, 70% and 80%), while combining different annealing temperatures (950, 1050 and 1150 °C) and soaking times (in the range of 20–180 s. The test results were organized using a data analysis and statistical tool, which was able to show the correlation between the different variables and the impacts of these on recrystallization and grain growth processes. For low treatment temperatures, the tested soaking times led to partial recrystallization, making this condition industrially unattractive. Instead, for the higher temperature, full recrystallization was achieved over a short time (20–40 s), depending on the reduction ratio. Regarding the grain growth behavior, it was found to be independent of the reduction ratio; for each treatment temperature, the grain growth showed a linear trend as a function of the soaking time only. Moreover, the static recrystallization kinetics were analyzed using a statistical analysis software program that was able to provide evidence indicating the most and least influential parameters in the process. In particular, taking into consideration the hardness values as output data, the temperature and soaking time were revealed to have major effects as compared with the reduction ratio, which was excluded from the statistical analysis. The prediction approach allowed us to formulate a regression equation in order to correlate the response and terms. Moreover, a response optimizer was used to predict the best solution to get as close as possible to the hardness target required by the market.

Keywords: AISI 904L; super-austenitic; stainless steel; corrosion resistance; mechanical properties; recrystallization; grain growth; thermomechanical treatment; efficiency of the production process

Citation: Stornelli, G.; Gaggiotti, M.; Mancini, S.; Napoli, G.; Rocchi, C.; Tirasso, C.; Di Schino, A. Recrystallization and Grain Growth of AISI 904L Super-Austenitic Stainless Steel: A Multivariate Regression Approach. *Metals* **2022**, *12*, 200. https://doi.org/10.3390/met12020200

Academic Editor: Wislei Riuper Osório

Received: 11 December 2021
Accepted: 18 January 2022
Published: 21 January 2022

1. Introduction

Austenitic stainless steels are employed in a very wide variety of fields, thanks to the combination they show in terms of their hardness, strength and ductility [1,2], meaning they are extremely formable and weldable [3,4]. The high temperature and general corrosion resistance, furthermore, allow many grades, such as AISI 304 and AISI 316L, to be employed

in a very large range of applications [5–7]. These steel grades are widely used in the automotive field, as they are able to satisfy the market requirements for weight and safety (e.g., [8–10]). Many applications are also found in the energy field, such as in oil and gas [11] and fuel cells [12].

In the early 1990s, the increasing demand for steels with superior mechanical properties, pushed by the need to operate in extremely severe environments, led to the birth of a new category of steels, called super-austenitic steels [13–15].

Compared to ordinary types of stainless steels, the super-austenitic ones are characterized by higher levels of some elements, such as chromium, nickel and molybdenum [16,17]. Thanks to the presence of the above elements, the material's capability to be applied in aggressive environments and in severe thermal conditions is strongly enhanced [18,19]. Further, improved performance in terms of mechanical strength compared to commercial austenitic stainless steel is reported for this class of materials [20,21].

AISI 904L is now one of the most common grades of this high-strength austenitic stainless steel (HSASS) [16] following its applications in energy [22,23], petrochemical [24,25] and marine sectors [26,27]. In particular, it is widely adopted in synthetic biomass ash environments [22], in oil and gas transportation [28] and in components employed in seawater environments [29,30].

This is mainly related to its excellent pitting and intergranular corrosion resistance [20,31,32], high strength [17] and high temperature resistance [33,34]. The latter is in great demand by many customers.

One of the main limits related to AISI 904L steel is the manufacturing cost, due to the high nickel and molybdenum contents, resulting in the material's high price compared to similar steel grades [1]. Moreover, the precipitation of the sigma (σ) phase [20,35] and the characteristic refractoriness [36] represent technological limitations for industrial production. The phenomenon of σ phase precipitation in austenitic and super-austenitic stainless steels occurs over a temperature range of 600 to 1000 °C [35]. The σ phase increases with increasing time and temperature; for this reason, the material is susceptible to crack generation during the hot deformation process [15,37,38]. At the same time, the refractoriness plays an important role during the annealing treatment [18]. The difficulties involved in dissipating heat, or in contrast in obtaining a thick and homogeneous material, create a lot of trouble during the heating process and the hot plastic deformation of AISI 904L [18,37,39].

In the literature, several studies are reported related to the microstructural evolution of AISI 904L, particularly focused on plastic deformation (e.g., [40–42]). Numerous variables have heavy impacts during this mechanical process and the consequent thermal treatments, so much that their effect needs to be analyzed in depth.

Generally, it is well known that the strengthening properties of austenitic stainless steels are strongly affected by the chemical composition and microstructural features [43,44]. Moreover, it is also known that the conventional hardening and tempering treatments that is typically used to improve the mechanical performances of other steel grades (such as ferritic–martensitic [45,46] or maraging steels [47]) are not effective on austenitic stainless steels. On the contrary, cold rolling and subsequent heat treatment is a very effective method for grain size refinement [48], consequentially leading to an increase in the mechanical properties of austenitic stainless steels [49,50]. The work-hardening behavior of steels after the cold rolling process is heavily dependent on the amount of stored energy in the material during the process. As the cold reduction ratios increase, the dislocation density increases and the microstructure progressively changes. During the subsequent annealing heat treatment, following the work-hardening induced by the deformation process, primary recrystallization and grain growth phenomena occur, depending on the heat treatment temperature and soaking time [51,52]. The grain growth phenomena typically act in two modes: (I) normal grain growth (NGG) with a uniform increase in grain size, based on grain boundary migration and annihilation of slam grains; (II) abnormal grain growth

(AGG) or secondary recrystallization, characterized by the rapid growth of some grains at the expense of neighboring ones (e.g., [53,54]).

Many studies have aimed to investigate the effects of the cold rolling process on the recrystallization of austenitic stainless steels [55–57]. Belyakov et al. [51] investigated a static restoration mechanism operating during annealing on AISI 304 stainless steel. Their analysis showed that the annealing treatment is characterized by recovery, transient recrystallization and normal grain growth; in the first phase of annealing, recovery developed quickly at the grain boundaries, leading to a fast release of high internal stresses, after which a rapid grain growth phenomenon occurs. Finally, their analysis showed a large fraction of annealing twins in a fully recrystallized state. Di Schino et al. reported on the recrystallization behavior of AISI 316 [58], AISI 301 [59] and low-nickel austenitic stainless steels [60]. Other studies referring to super-austenitic stainless steel have not yet been fully consolidated.

Within this framework, in this paper the recrystallization and grain growth behavior of AISI 904L super-austenitic stainless steel is reported as a function of the thermomechanical parameters. The evolution of the microstructure and hardness of steel after cold rolling and subsequent annealing treatment was analyzed with the aim of optimizing the thermomechanical treatment conditions and improving the efficiency of the production process, also by means of a multivariate regression approach [61–63]. The investigation involved three different cold reduction ratios (50%, 70% and 80%), combining different annealing temperatures (950 °C, 1050 °C and 1150 °C) and soaking times in the range of 20–180 s. The execution of the experiments was managed through the use of a data analysis and statistical tool, which was able to show the correlation between the various process variables and the impacts of these on the recrystallization and grain growth processes. Considering the hardness target as required by the market, process parameters were established and optimized for industrial applications based on a multivariate approach.

2. Materials and Methods

The nominal steel chemical composition of AISI 904L considered in this work, according to the normative UNI EN 10088, is shown in Table 1.

Table 1. Nominal chemical composition of AISI 904L steel (wt. %) (Fe to balance).

C	Mn	Si	Cr	Ni	Mo	N	Cu
≤0.02	≤2.00	≤0.70	19.00–21.00	24.00–26.00	4.00–5.00	≤0.15	1.30–2.00

The material was cold-worked according to three different cold rolling ratios (CR). After cold rolling, the material was heat-treated in an electric resistance oven (FM-77/H), at three different heating temperatures. The time evolution was considered at different temperatures while varying the soaking time (Table 2). After maintaining target treatment conditions, the samples were immediately cooled in water.

After heat treatment, the specimens were etched in a HNO_3 + H_2O solution in an electrolytic cell using AISI 316L as the cathode. The microstructure was then analyzed using a light microscope (Eclipse LV150 NL, Nikon, Tokyo, Japan), and for the fully recrystallized samples, image analysis was performed using dedicated software (AlexaSoft, X-Plus, serial number: 6308919690486393, Florence, Italy). From the image analysis, it was possible to determine and compare the average grain size of AISI 904L steel as a function of the thermomechanical conditions.

The hardness was measured using a Vickers durometer (HV-50, Remet, Bologna, Italy) with a 1 Kg load at $\frac{1}{4}$ of the thickness. Three indentations were carried out for each specimen and the average value was considered.

Table 2. Thermomechanical conditions of the considered samples.

Cold Rolling Ratios (CR)	Soaking Time
Annealing Temperature: 1150 °C	
80%—70%—50%	20 s 40 s 60 s 80 s 100 s 120 s
Annealing temperature: 1050 °C	
80%—70%—50%	20 s 40 s 60 s 80 s 100 s 120 s
Annealing temperature: 950 °C	
80%—70%—50%	30 s 60 s 90 s 120 s 150 s 180 s

The recrystallized volume fraction (X_v) was evaluated starting from the hardness measurements according to Equation (1) based on [60]:

$$X_v = \frac{\delta^2(t) - \delta_C^2}{\delta_R^2 - \delta_C^2} \quad (1)$$

where X_v = recrystallized volume fraction; $\delta(t)$ = hardness value at specific soaking time; δ_c = hardness value of deformed material at specific reduction ratio; δ_R = hardness value of fully recrystallized material.

The results were analyzed using a data analysis and statistical tool. Such analyses provide evidence of the effects of the different process parameters on the microstructural evolution (cold rolling ratio, annealing temperature, soaking time). The first variable was studied at 3 levels, while the annealing temperature was studied at 2 and the soaking time at 6 levels.

3. Results and Discussion

3.1. Deformed Material

The microstructure of the material, prior to cold rolling, is reported in Figure 1.

Figure 1 shows a fully recrystallized material characterized by a homogeneous structure dominated by equiaxic grains. The cold-rolled material's microstructure evolution with increasing deformation rate is reported in Figure 2. This microstructure evolution leads to the work-hardening behavior reported in Figure 3 in terms of hardness.

3.2. Recrystallization Behavior

The effects of heat treatment parameters (temperature and soaking time) on the hardness values (HV_1) and recrystallization volume fraction (X_v) of AISI 904L steel after cold rolling down to 50% and annealing are reported in Figure 4a,b, respectively. It is worth noting that an annealing temperature of 950 °C is not sufficient to achieve full recrystallization after 180 s. The progressively decreasing trend of hardness values suggests that for longer soaking times, the materials would reach complete recrystallization. However, times longer than 180 s are industrially unattractive. Starting from hardness measurements and based on Equation (1), the recrystallized volume fraction was calculated for 50% cold-rolled steel as a function of the heat treatment conditions (Figure 4b). It is clearly visible that while

for temperatures of 1050 °C and 1150 °C 100% recrystallization is achieved in 20–40 s, the maximum recrystallization fraction reached at 950 °C is about 90%. From the micrographic analysis, as indicated by red arrows in Figure 5, areas with partial recrystallization are clearly visible. On the other hand, a fully recrystallized microstructure is achieved at higher temperatures (both 1050 °C and 1150 °C) at times ranging 20–40 s (Figure 6). The grain size distribution obtained from the image analysis relative to the samples in Figure 6 is shown in Figure 7.

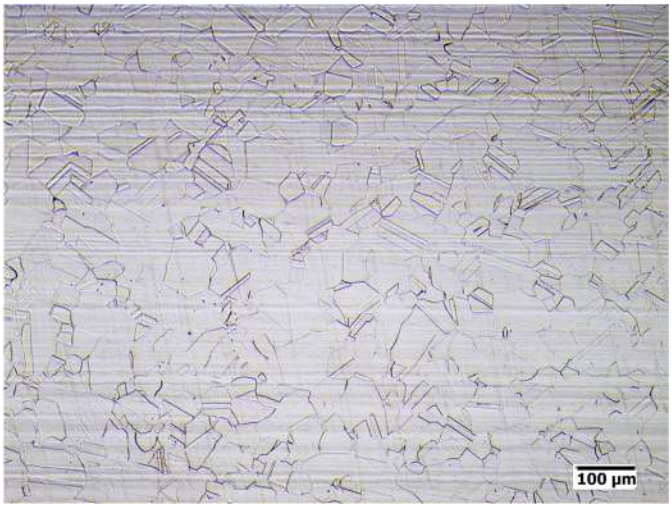

Figure 1. AISI 904L specimen prior to cold rolling process (starting material).

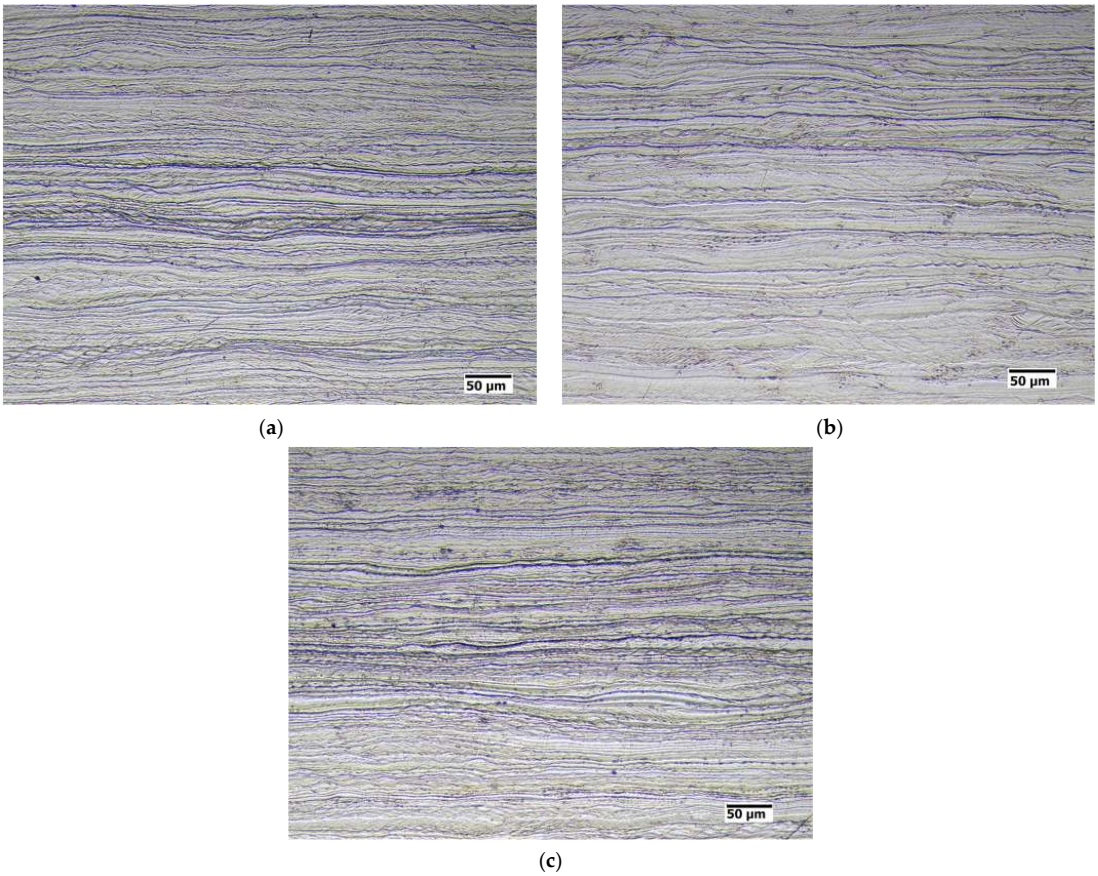

(**a**) (**b**)

(**c**)

Figure 2. AISI 904L cold-rolled steel. (**a**) CR: 50%; (**b**) CR: 70%; (**c**) CR: 80%.

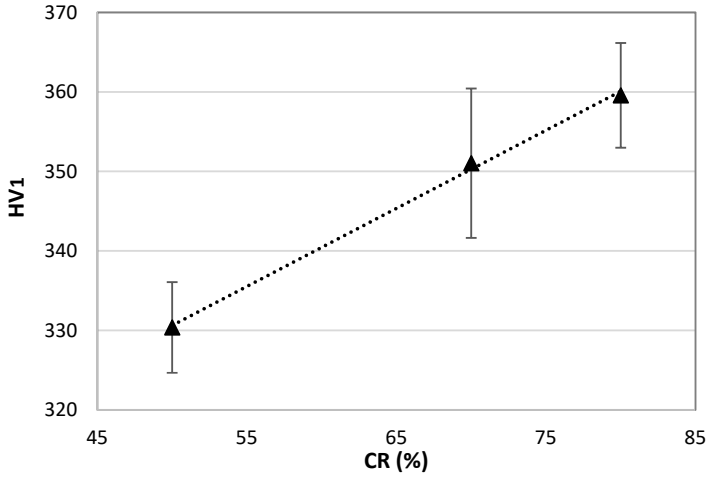

Figure 3. Hardening behavior of the AISI 904L steel.

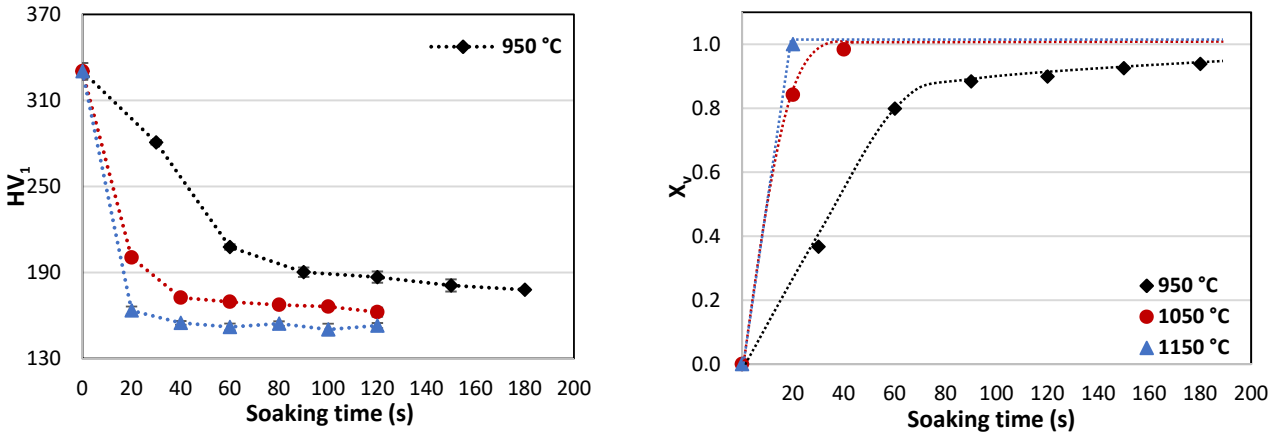

(**a**) (**b**)

Figure 4. Effects of process parameters (temperature and soaking time) on hardness values (HV_1) (**a**) and recrystallized volume fraction (X_v) (**b**) of AISI 904L cold-rolled at 50%.

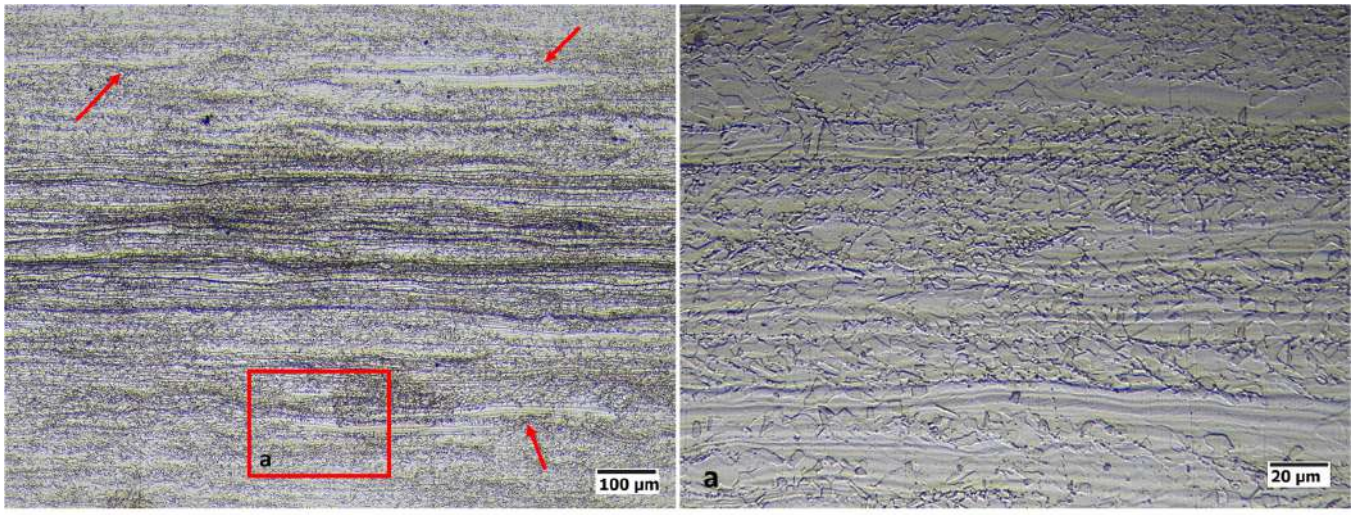

Figure 5. AISI 904L steel after cold rolling at 50% and annealing at 950 °C for 180 s (red arrows indicate the partially recrystallized areas).

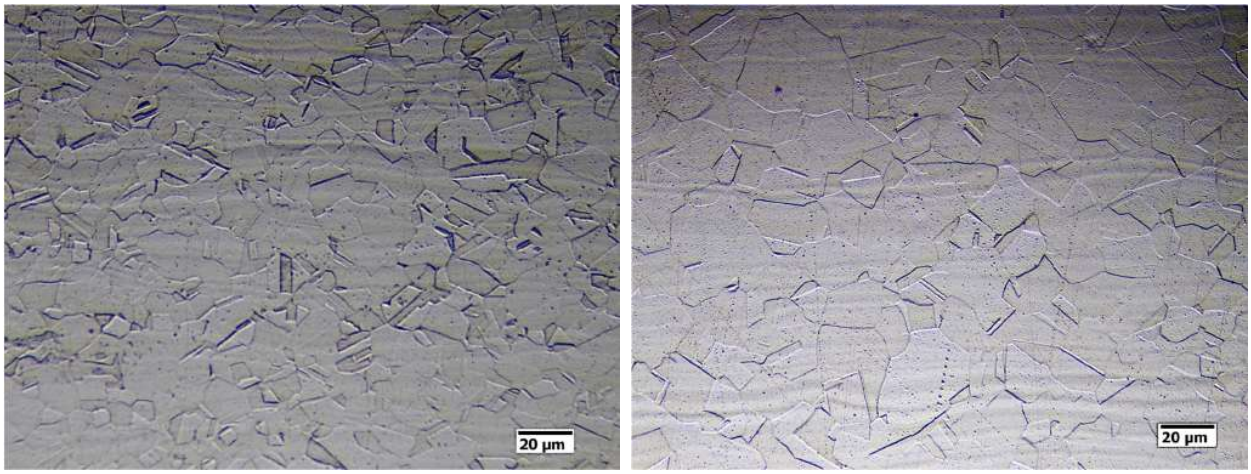

(**a**) (**b**)

Figure 6. AISI 904L steel after cold rolling at 50% and annealing at (**a**) 1050 °C for 40 s and (**b**) 1150 °C for 20 s.

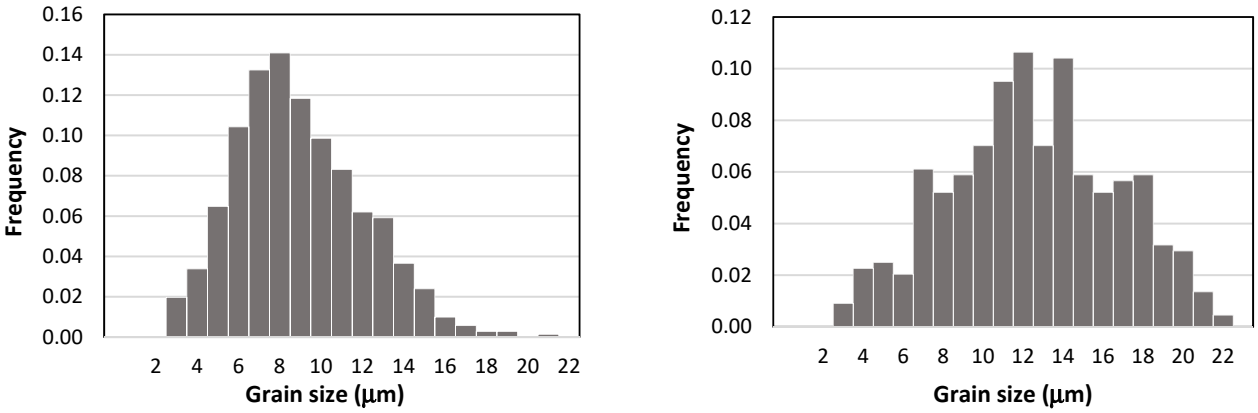

Count: 710	Max: 21.2 µm
Average: 9.5 µm	Min: 3.2 µm
StDev: 3.1 µm	Mode: 7.6 µm

(**a**)

Count: 442	Max: 22.9 µm
Average: 12.9 µm	Min: 3.5 µm
StDev: 4.2 µm	Mode: 8.5 µm

(**b**)

Figure 7. Grain size distribution of AISI 904L steel after cold rolling at 50% and annealing at (**a**) 1050 °C for 40 s and (**b**) 1150 °C for 20 s.

Similar results can be seen for higher deformation ratios (70% and 80%) (Figures 8–11). Additionally, at high cold reduction ratios, a 950 °C annealing temperature is not sufficient to fully recrystallize the material up to 180 s holding time (Figures 8–10). The maximum recrystallization volume fractions (Figures 8b and 10b) relating to the heat treatment at 950 °C for 180 s are about 94% and 97%, respectively, for the CR ratios of 70% and 80%. Likewise, for the treatment temperatures of 1050 °C and 1150 °C, a full recrystallization is achieved for the higher CR ratios. In particular, for the CR at 70%, as for CR at 50%, the complete recrystallization (Figure 8a) occurs over a range of soaking times of 20–40 s as a function of annealing temperature. As expected, the recrystallization kinetics speed up as the heat treatment temperature increases. The microstructures as achieved after full recrystallization of steel cold-rolled at 70% and treated at 1050 °C for 40 s and at 1150 °C for 20 s are reported in Figure 9. For the higher CR ratio (80%), it is not possible to distinguish the effects of temperature on the recrystallization behavior due to the higher energy stored during the cold rolling.

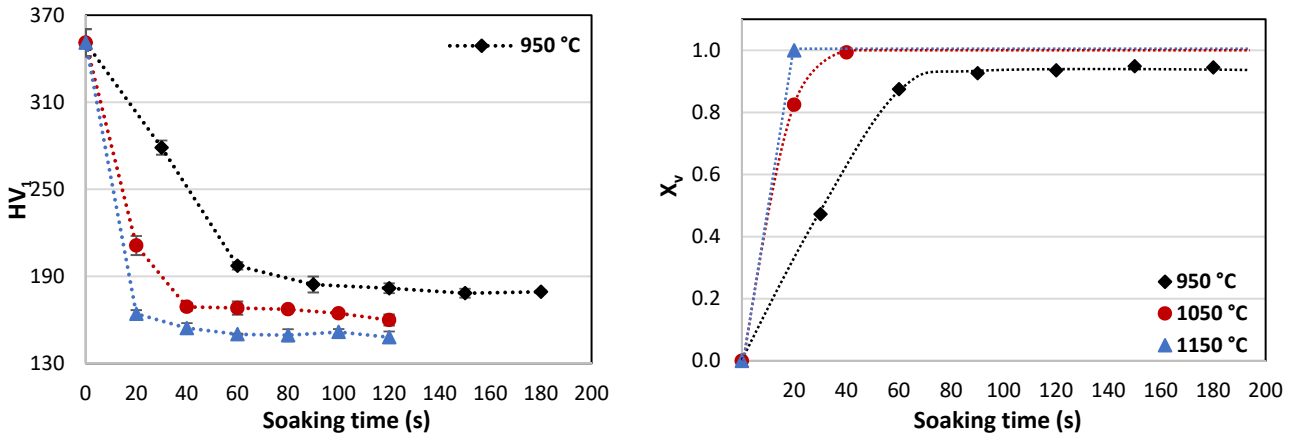

(**a**) (**b**)

Figure 8. Effects of process parameters (temperature and soaking time) on hardness values HV_1 (**a**) and the recrystallized volume fraction X_v (**b**) of AISI 904L cold-rolled at 70%.

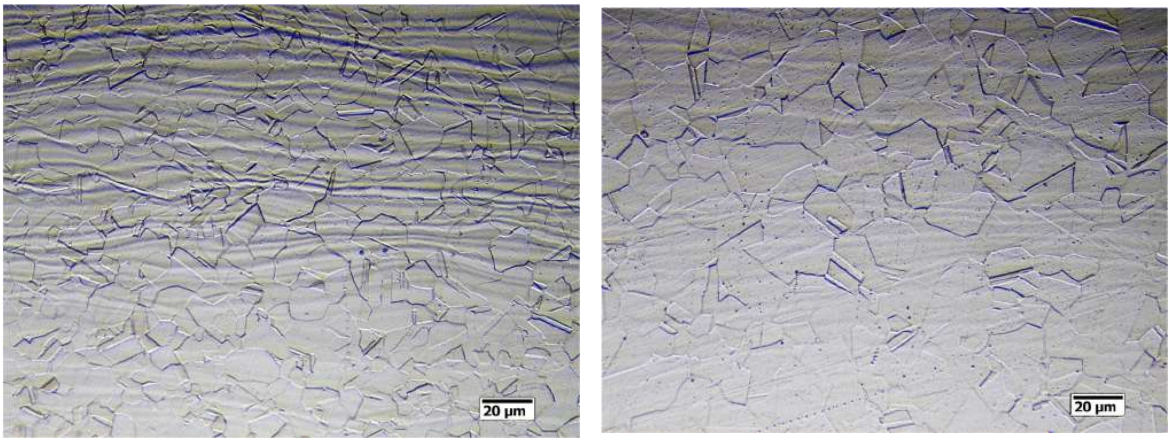

(**a**) (**b**)

Figure 9. AISI 904L steel after cold rolling at 70% and annealing at (**a**) 1050 °C for 40 s and (**b**) 1150 °C for 20 s.

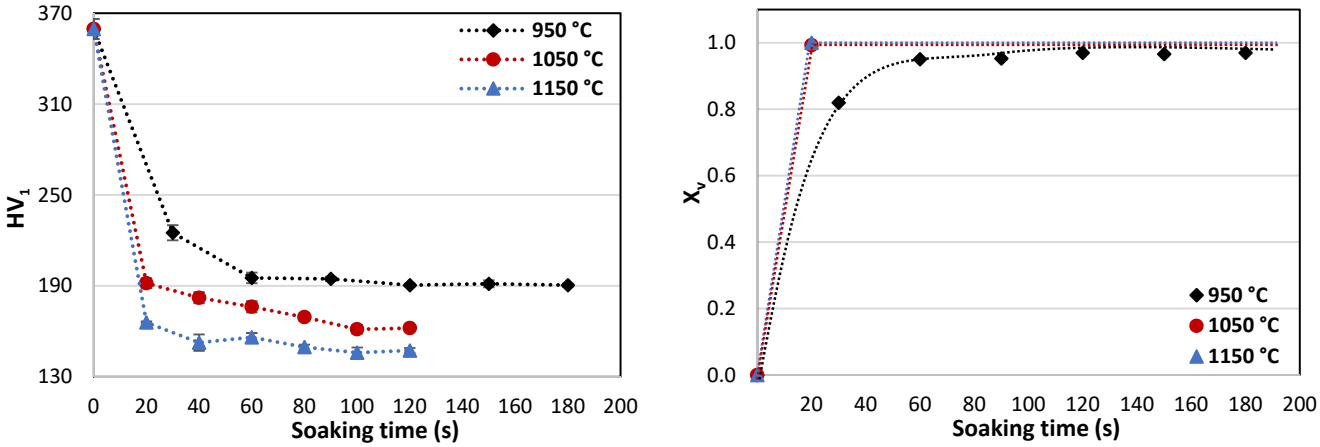

(**a**) (**b**)

Figure 10. Effects of process parameters (temperature and soaking time) on hardness values HV_1 (**a**) and recrystallized volume fraction X_v (**b**) of AISI 904L cold-rolled at 80%.

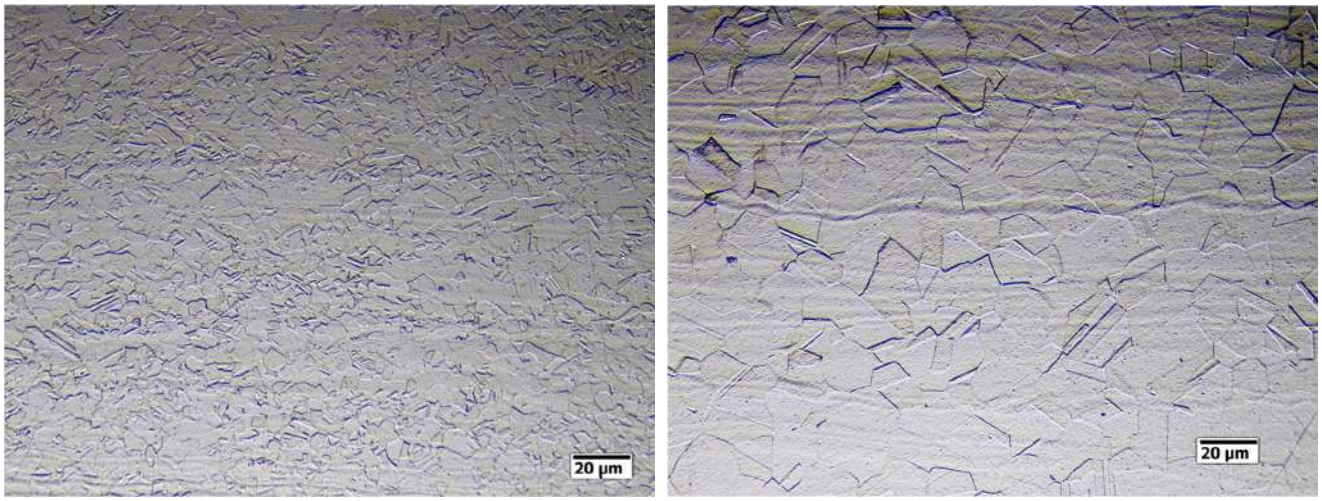

(**a**) (**b**)

Figure 11. AISI 904 steel after cold rolling at 80% and annealing at (**a**) 1050 °C for 20 s and (**b**) 1150 °C for 20 s.

After 20 s, the AISI 904L steel cold-rolled at 80% is fully crystalline at both 1050 °C and 1150 °C treatment temperatures. To confirm this statement, Figure 11 shows the microstructures, completely recrystallized, obtained after the annealing treatments for 20 s at 1050 °C and 1150 °C. The clear distinction between the two microstructures in Figure 11 is the grain size; for a very high CR ratio (80%) and with the same soaking time, a low treatment temperature (1050 °C) is sufficient to obtain a very fine microstructure. The results in terms of the average grain size obtained from the image analysis for the different considered cases are reported in Table 3 and clearly show that the finest microstructure is achieved after cold rolling at 80% and annealing at 1050 °C for 20 s.

Table 3. The average grain size for the recrystallized material for different process parameters.

Annealing Temperature (°C)	Recrystallization Time (s)	Mean G.S. (µm)	St. Dev (µm)	Mode (µm)
Cold rolling ratios (CR) at 50%				
1050	40	9.5	3.1	7.6
1150	20	12.9	4.2	8.5
Cold rolling ratios (CR) at 70%				
1050	40	9.3	3.1	4.3
1150	20	14.4	4.5	11.2
Cold rolling ratios (CR) at 80%				
1050	20	4.1	1.3	2.8
1150	20	14.5	4.5	19.9

3.3. Grain Growth Behavior

Grain growth phenomena after full recrystallization in AISI 904L were evaluated by quantifying the average grain size dependence on the process parameters (CR, temperature and soaking time). The results in terms of the grain size evolution as a function of the soaking time at annealing temperatures of 1050 and 1150 °C are reported in Figure 12. Moreover, the relevant microstructures are shown in Figures 13 and 14. The results show that the average grain size increases with increasing heat treatment temperature and soaking time and is independent of the cold rolling ratio. Furthermore, for each temperature, the grain size grows linearly as a function of the soaking time.

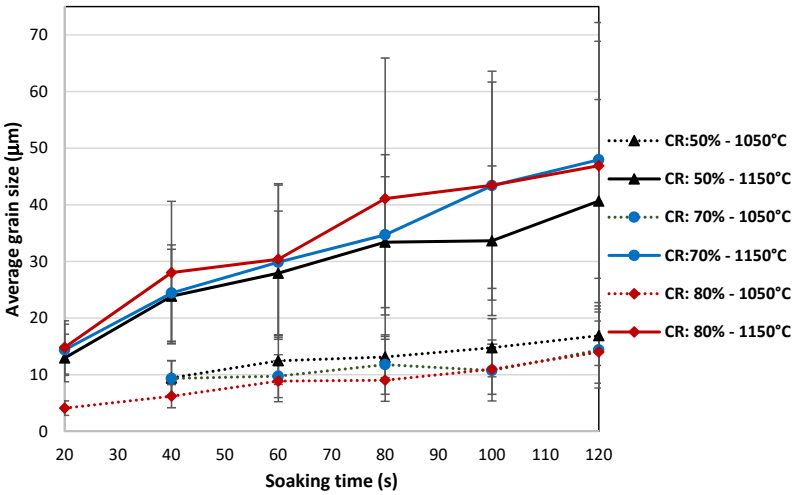

Figure 12. Grain size evolution with process parameters in AISI 904L stainless steel.

As shown in Figure 12 and in the microstructural evolution in Figure 13, no significative grain growth can be observed at 1050 °C for any of the treatment times tested. At 1150 °C (Figure 14), the grain growth at high temperature is evident for short treatment times; already after 40 s of heat treatment at 1150 °C, the average grain size is almost double the maximum value at 1050 °C after 120 s. Therefore, the grain growth kinetics of AISI 904L super-austenitic stainless steel are strongly intensified by the temperature and less so by the soaking time. Indeed, it is well known that the grain growth kinetics depend on the grain boundary migration, and hence the atomic diffusion [53]. Furthermore, at high temperatures (about 1100 °C for austenitic stainless steels [64]), the Zener pinning of the grain boundaries is mitigated by the dissolution or coarsening of the precipitates [65].

3.4. Statistical Analysis

The statistical analysis of annealing process data, obtained by setting the different reduction ratios, temperatures and soaking time conditions, was performed using the design of experiments (DOE) approach. This is the most popular statistical technique for the design of tests and is useful for reducing the process organization time while providing greater reliability in the results. To reduce the complexity of the study, due to the differences in soaking times for the temperature of 950 °C compared to 1050 °C and 1150 °C, the analysis was performed by considering only the last two annealing temperatures, along with their respective reduction ratios and soaking times. The objective was to evaluate the influence of the variables involved during the annealing process through the microstructure and laboratory testing and then to compare them with the solutions made available using the statistical analysis software Minitab. The first step was to associate each treatment condition with the respective hardness value (as discussed in Section 2) in such a way as to create a database with the input–output data. Then, the general linear model (GLM), a useful framework for comparing how several variables affect the process, was chosen due to the presence of a large number of levels associated with the three different considered parameters. The GLM is the foundation for several statistical tests, including the analysis of variance (ANOVA) approach, the technique used in this case. The first step of a variance analysis is the setting of a proper null hypothesis (H_0), a statement assumed true until there is clear evidence to the contrary. In this study, H_0 refers to the parameters involved regarding their great influence (or lack thereof) on the annealing process and related recrystallization phenomena. Below, the variables involved are listed, as mentioned in Section 2:

- A: Temperature;
- B: Reduction ratio;
- C: Soaking time.

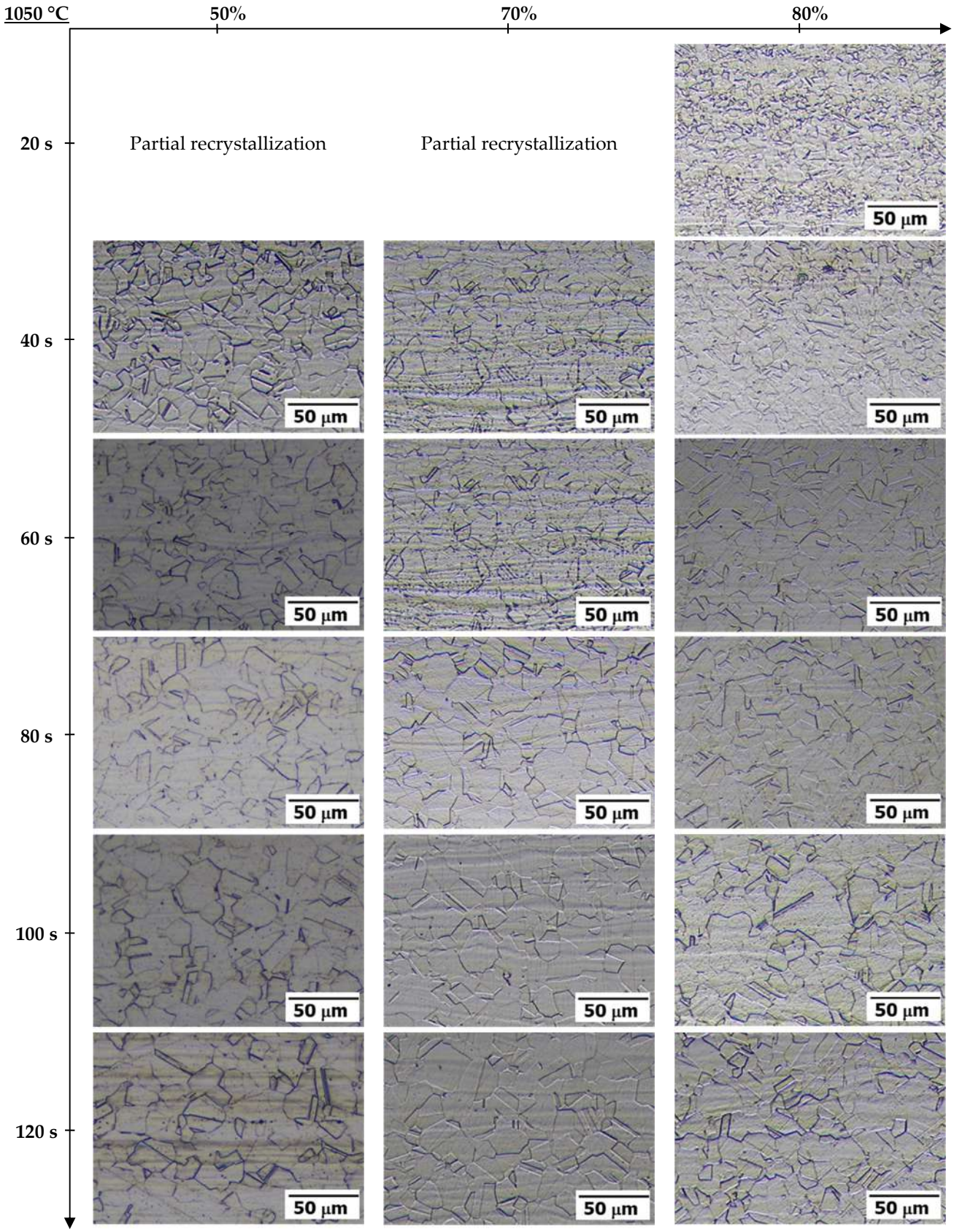

Figure 13. Grain growth evolution in AISI 904L as a function of the cold rolling ratio (CR: 50%, 70%, 80%) after annealing treatment at 1050 °C and soaking times in the range of 20–120 s.

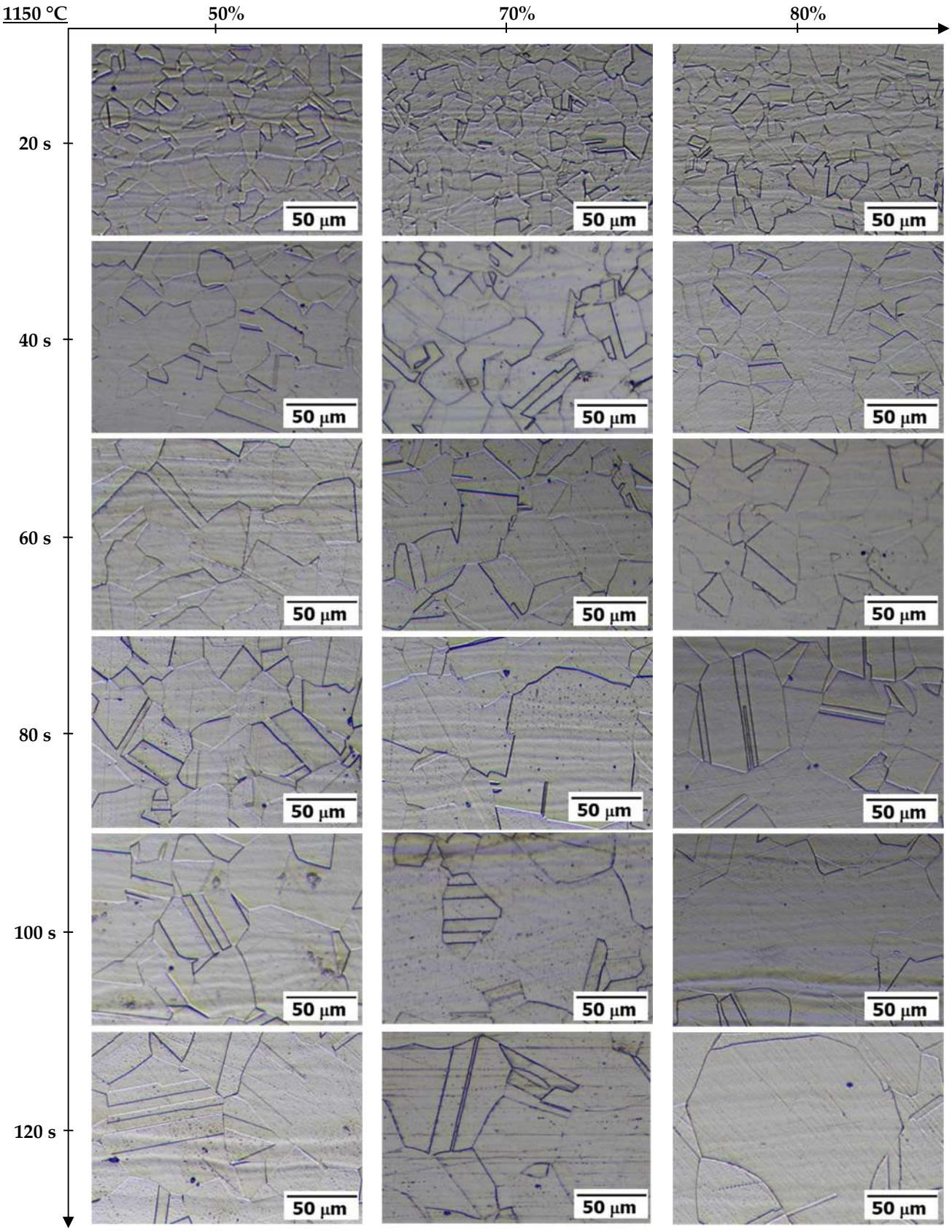

Figure 14. Grain growth evolution in AISI 904L as a function of the cold rolling ratio (CR: 50%, 70%, 80%) after annealing treatment at 1150 °C and soaking times in the range of 20–120 s.

The GLM allows one to evaluate the influence of individual parameters, as well as the influence of their interactions (double interaction in this case study). The results of the analysis are shown in Figure 15. By looking at the Pareto chart, it is easy to understand which parameters have a greater effect according to the software. The interpretation of *p*–value coefficients, therefore, confirms the assessments referred to in the graph, with the *p*-value being defined as the probability of obtaining results at least as extreme as the observed results of a statistical hypothesis test. A smaller *p*-value means that there is stronger evidence in favor of the alternative hypothesis. In particular, for $p > 0.05$ (called the level of significance), the probability of error in not considering a variable is considered low. Otherwise, if the *p*-value is lower than 0.05, the parameter must be considered in the analysis and is relevant for the process. The *p*-values associated with the parameters and their interactions are shown in Table 4. Referring to the condition expressed above, the reduction ratio (B), the temperature–reduction ratio (AB) and the soaking time–reduction ratio (BC) show values higher than 0.05, meaning they can be removed from the analysis.

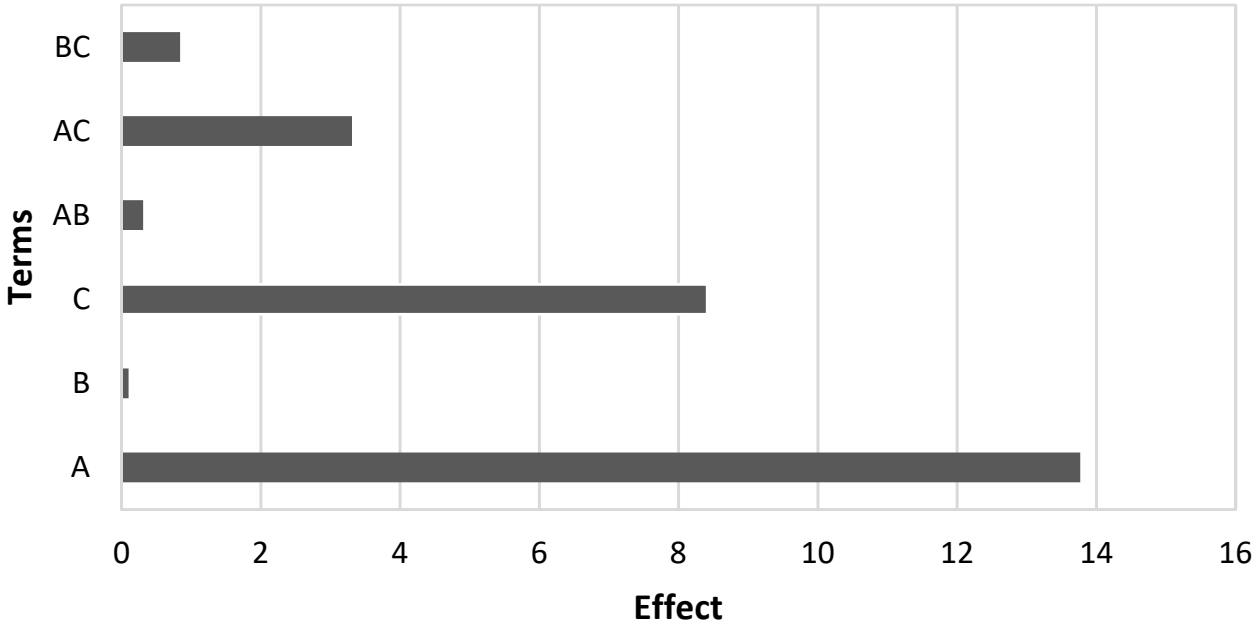

Figure 15. Effects of different test parameters and interactions, computed using Minitab software.

Table 4. The *p*-values for different parameters and interactions.

Terms	*p*-Value
A	0.00
B	0.917
C	0
AB	0.761
BC	0.418
AC	0.008

As expected, the temperature and soaking time are the terms with a meaningful effect on the process, which is in accordance with the results obtained through laboratory analysis. During an annealing process, a higher treatment temperature and a longer soaking time will affect the hardness of the material, as shown in Figure 16.

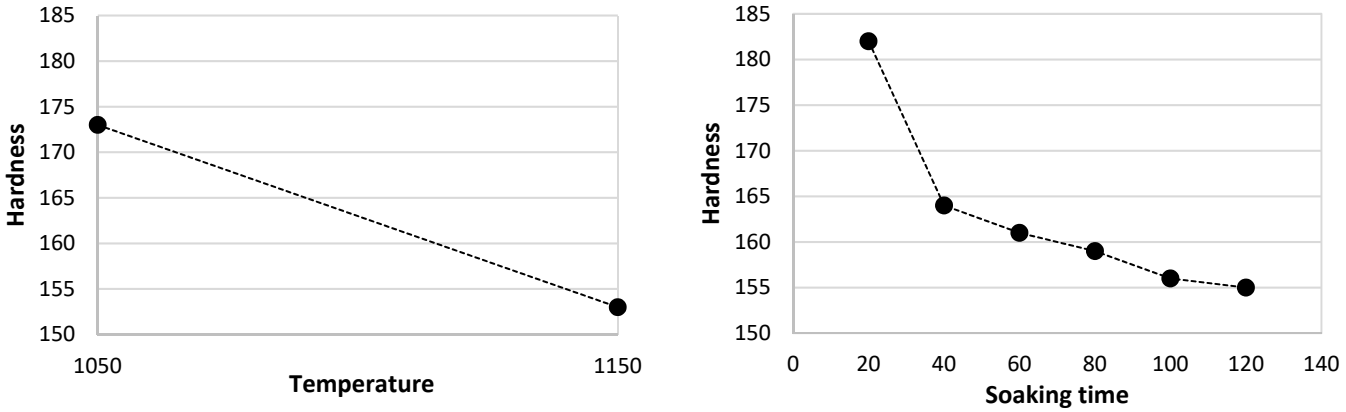

Figure 16. Effects of temperature and soaking time on hardness, computed using Minitab software.

The above analysis allowed us to formulate the following regression Equation (2):

$$\begin{aligned}\text{Hardness} = \; & 163.444 + 9.959 * \left(1050\,^{\circ}\text{C}\right) - 9.959 * \left(1150\,^{\circ}\text{C}\right) + 19.37 * (20\,\text{s}) \\ & + 0.77 * (40\,\text{s}) - 1.46 * (60\,\text{s}) - 3.89 * (80\,\text{s}) - 6.80 \\ & * (100\,\text{s}) - 7.99 * (120\,\text{s}) + 8.36 * \left(1050\,^{\circ}\text{C}\right) * (20\,\text{s}) + 0.35 \\ & * \left(1050\,^{\circ}\text{C}\right) * (40\,\text{s}) - 0.67 * \left(1050\,^{\circ}\text{C}\right) * (60\,\text{s}) - 1.50 \\ & * \left(1050\,^{\circ}\text{C}\right) * (80\,\text{s}) - 2.59 * \left(1050\,^{\circ}\text{C}\right) * (100\,\text{s}) - 3.94 \\ & * \left(1050\,^{\circ}\text{C}\right) * (120\,\text{s}) - 8.36 * \left(1150\,^{\circ}\text{C}\right) * (20\,\text{s}) - 0.35 \\ & * \left(1150\,^{\circ}\text{C}\right) * (40\,\text{s}) + 0.67 * \left(1150\,^{\circ}\text{C}\right) * (60\,\text{s}) + 1.50 \\ & * \left(1150\,^{\circ}\text{C}\right) * (80\,\text{s}) + 2.59 * \left(1150\,^{\circ}\text{C}\right) * (100\,\text{s}) + 3.94 \\ & * \left(1150\,^{\circ}\text{C}\right) * (120\,\text{s})\end{aligned} \tag{2}$$

The level of reliability associated with this regression equation can be measured through an indicator defined as the coefficient of determination (R-sq), which in this case is equal to 94%.

Considering the hardness target value imposed by the market (around 160 Vickers), the response optimizer tool allows us to set the values of the different parameters involved in such a way as to obtain the required result. In this way, Minitab calculates an optimal solution by identifying the combination of input variable settings (Table 5).

Table 5. Solution proposed by Minitab software to obtain the hardness target of 160 Vickers.

Temperature	Soaking Time	Hardness Fit	Composite Desirability
1050 °C	120 s	161,47	97%

The "hardness fit" represents the hardness value to be reached by setting the temperature and soaking time to 1050 °C and 120 s. This value is very close to the target; the slight difference is justified by the term "composite desirability", which can be considered as a parameter of the response optimizer accuracy. The prediction approach in this way allows us to exclude from the analysis the parameters and the combination of terms not relevant in the process, providing a solution that is as close as possible to the required hardness target.

4. Conclusions

The recrystallization and grain growth behavior of AISI 904 L steel have been reported here as functions of the thermomechanical parameters (cold reduction ratio and heat treatment conditions).

The results are summarized below:

1. Soaking at 950 °C did not appear to be effective in achieving a fully recrystallized fraction;
2. Steel fully recrystallized after soaking at 1050 °C and 1150 °C;

3. Soaking at 1050 °C was shown to be the best condition in terms of grain size refinement;
4. For the cold rolling ratios of 50% and 70%, a strong temperature effect was detected. In particular, the recrystallization process appeared to be fastest at 1150 °C with respect to the lower annealing temperature;
5. For the cold rolling ratio of 80%, the difference in terms of the recrystallization rates exerted by both 1050 °C and 1150 °C was negligible, following the high energy storage related to the heavy reduction ratio;
6. Grain growth phenomena after full recrystallization for treatment temperatures of 1050 °C and 1150 °C showed a linear trend as a function of the treatment time, independently of the cold reduction ratio. A slight increase in grain size was observed at 1050 °C for each treatment time tested. Otherwise, at 1150 °C, significant grain growth occurred within short soaking times;
7. As expected, the results from a statistical analysis based on GLM confirmed that the temperature and soaking time are the factors that have meaningful effects on the process.

For the first time, the thermal–mechanical treatment of AISI 904L steel was comprehensively studied. Evidence from a laboratory analysis in terms of the most relevant thermomechanical parameters in the process was confirmed using a predictive approach. This was established in the form of an equation with a coefficient of determination of 94% and a response optimizer with a given accuracy of 97%, which allowed us to specify a solution for hardness target demands. The further development of this theme is justified by the increasingly specific customer requirements, and it might be possible to apply this approach to other steels and specific market demands.

Author Contributions: Conceptualization, G.S., G.N. and A.D.S.; methodology M.G., G.S., S.M. and C.T.; formal analysis, M.G., G.S. and G.N.; investigation, M.G. and G.S.; writing—original draft preparation, M.G., G.S. and G.N.; writing—review and editing, all authors; supervision, G.N., C.R. and A.D.S. All authors have read and agreed to the published version of the manuscript.

Funding: This research received no external funding.

Institutional Review Board Statement: Not applicable.

Informed Consent Statement: Not applicable.

Data Availability Statement: The data presented in this study are available on request from the corresponding author.

Acknowledgments: The authors are grateful to Arianna Lamperini, Elena Petrucci and Federico Virili of the Industrial Engineering Course at University of Perugia (Terni branch) for assistance in samples preparation and metallographic analysis.

Conflicts of Interest: The authors declare no conflict of interest.

References

1. Bradaskja, B.; Pirnar, B.; Fazarinc, M.; Fajfar, P. Deformation behaviour and microstructural evolution during hot compression of AISI 904L. *Steel Res. Int.* **2011**, *82*, 346–351. [CrossRef]
2. Zhang, Y.; Li, M.; Bi, H.; Gu, J.; Chen, D.; Chang, E.; Zhang, W. Martensite transformation behavior and mechanical properties of cold-rolled metastable Cr-Mn-Ni-N austenitic stainless steels. *Mater. Sci. Eng. A* **2018**, *724*, 411–420. [CrossRef]
3. Painkra, T.K.; Naik, K.S.; Nishad, R.K.; Sen, P.K. Review about high performance of Austenitic Stainless Steel. *Int. J. Innov. Res. Sci. Technol.* **2014**, *1*, 93–99.
4. Brooks, J.A. Weldability of High N, High Mn Austenitic Stainless Steel. *Weld. J.* **1975**, *54*, 189–195.
5. Song, R.B.; Xiang, J.Y.; Hou, D.P. Characteristics of mechanical properties and microstructure for 316L austenitic stainless steel. *J. Iron Steel Res. Int.* **2011**, *18*, 53–59. [CrossRef]
6. Al-Mangour, B.; Mongrain, R.; Irissou, E.; Yue, S. Improving the strength and corrosion resistance of 316L stainless steel for biomedical applications using cold spray. *Surf. Coatings Technol.* **2013**, *216*, 297–307. [CrossRef]
7. Martínez, T.L.M.; Sanz, O.; Domínguez, M.I.; Centeno, M.A.; Odriozola, J.A. AISI 304 Austenitic stainless steels monoliths for catalytic applications. *Chem. Eng. J.* **2009**, *148*, 191–200. [CrossRef]

8. Santacreu, P.-O.; Glez, J.-C.; Chinouilh, G.; Fröhlich, T. Behaviour Model of Austenitic Stainless Steels for Automotive Structural Parts. *Steel Res. Int.* **2006**, *77*, 686–691. [CrossRef]
9. Di Schino, A. Manufacturing and Applications of Stainless Steels. *Metals* **2020**, *10*, 327. [CrossRef]
10. Rufini, R.; Di Pietro, O.; Di Schino, A. Predictive simulation of plastic processing of welded stainless steel pipes. *Metals* **2018**, *8*, 519. [CrossRef]
11. Di Schino, A.; Testani, C. Corrosion behavior and mechanical properties of AISI 316 stainless steel clad Q235 plate. *Metals* **2020**, *10*, 552. [CrossRef]
12. Sharma, D.K.; Filipponi, M.; Di Schino, A.; Rossi, F.; Castaldi, J. Corrosion behaviour of high temperature fuel cells: Issues for materials selection. *Metalurgija* **2019**, *58*, 347–351.
13. Lewis, A.C.; Bingert, J.F.; Rowenhorst, D.J.; Gupta, A.; Geltmacher, A.B.; Spanos, G. Two- and three-dimensional microstructural characterization of a super-austenitic stainless steel. *Mater. Sci. Eng. A* **2006**, *418*, 11–18. [CrossRef]
14. Lo, K.H.; Shek, C.H.; Lai, J.K.L. Recent developments in stainless steels. *Mater. Sci. Eng. R Rep.* **2009**, *65*, 39–104. [CrossRef]
15. Jorge, J.C.F.; Meira, O.G.; Madalena, F.C.A.; de Souza, L.F.G.; Araujo, L.S.; Mendes, M.C. Evaluation of the AISI 904L Alloy Weld Overlays Obtained by GMAW and Electro-Slag Welding Processes. *J. Mater. Eng. Perform.* **2017**, *26*, 2204–2212. [CrossRef]
16. IMOA. *I.M.A. Practical Guidelines for the Fabrication of Duplex Stainless Steels*; International Molybdenum Association: London, UK, 2009; ISBN 9781907470004.
17. Zambon, A.; Ferro, P.; Bonollo, F. Microstructural, compositional and residual stress evaluation of CO2 laser welded super-austenitic AISI 904L stainless steel. *Mater. Sci. Eng. A* **2006**, *424*, 117–127. [CrossRef]
18. Tehovnik, F.; Žužek, B.; Arh, B.; Burja, J.; Podgornik, B. Hot rolling of the superaustenitic stainless steel AISI 904L. *Mater. Tehnol.* **2014**, *48*, 137–140.
19. Isaac Samuel, E.; Choudhary, B.K. Universal scaling of work hardening parameters in type 316L(N) stainless steel. *Mater. Sci. Eng. A* **2010**, *527*, 7457–7460. [CrossRef]
20. Devendranath Ramkumar, K.; Dagur, A.H.; Kartha, A.A.; Subodh, M.A.; Vishnu, C.; Arun, D.; Giridharan Vijay Kumar, M.; Abraham, W.S.; Chatterjee, A.; Abraham, J.; et al. Microstructure, mechanical properties and biocorrosion behavior of dissimilar welds of AISI 904L and UNS S32750. *J. Manuf. Process.* **2017**, *30*, 27–40. [CrossRef]
21. Nage, D.D.; Raja, V.S.; Raman, R. Effect of nitrogen addition on the microstructure and mechanical behavior of 317L and 904L austenitic stainless steel welds. *J. Mater. Sci.* **2006**, *41*, 2097–2112. [CrossRef]
22. Singh, M.K.; Mahobia, G.S.; Sinha, O.P.; Singh, V. Effect of synthetic biomass ash on high temperature corrosion behavior of super austenitic stainless steel 904L. *Mater. Res. Express* **2019**, *6*, 0965d3. [CrossRef]
23. Di Blasi, A.; Andaloro, L.; Siracusano, S.; Briguglio, N.; Brunaccini, G.; Stassi, A.; Aricò, A.S.; Antonucci, V. Evaluation of materials and components degradation of a PEM electrolyzer for marine applications. *Int. J. Hydrogen Energy* **2013**, *38*, 7612–7615. [CrossRef]
24. Barbosa, B.A.R.S.; Tavares, S.S.M.; Cobuci, A.; De MacÊdo, M.C.S. Influence of microstructure on pitting corrosion resistance of alloy 904L superaustenitic stainless steel. *Corrosion* **2012**, *68*, 739–746. [CrossRef]
25. Kangas, P.; Chai, G.C. Use of advanced austenitic and duplex stainless steels for applications in oil & gas and process industry. *Adv. Mater. Res.* **2013**, *794*, 645–669. [CrossRef]
26. Rohith, K.; Shreyas, S.; Vishnu Appaiah, K.B.; Sheshank, R.V.; Ganesha, B.B.; Vinod, B. Recent material advancement for marine application. *Mater. Today Proc.* **2019**, *18*, 4854–4859. [CrossRef]
27. Malik, A.U.; Ahmad, S.; Andijani, I.; Al-Fouzan, S. Corrosion behavior of steels in Gulf seawater environment. *Desalination* **1999**, *123*, 205–213. [CrossRef]
28. Koppula, S.; Gautam Jagarlamudi, V.; Sai Prudhvi, R.; Rajkumar, A.; Prashanth, S.; Saranya, J.; Sateesh, N.; Subbiah, R. Investigation of AISI 904L austenitic stainless steel by carbonitriding process under dry sliding conditions. *Mater. Today Proc.* **2021**, *44*, 1418–1422. [CrossRef]
29. Yang, D.; Huang, Y.; Peng, P.; Liu, X.; Zhang, B. Passivation behavior and corrosion resistance of 904L austenitic stainless steels in static seawater. *Int. J. Electrochem. Sci.* **2019**, *14*, 6133–6146. [CrossRef]
30. Ahmad, S.; Malik, A.U. Corrosion behaviour of some stainless steels in chlorinated Gulf seawater. *J. Appl. Electrochem.* **2001**, *31*, 1009–1016. [CrossRef]
31. Wang, J.; Shi, W.; Xiang, S.; Ballinger, R.G. Study of the corrosion behaviour of sensitized 904L austenitic stainless steel in Cl-solution. *Corros. Sci.* **2021**, *181*, 109234. [CrossRef]
32. Ramkumar, K.D.; Prabu, S.S.; Arivazhagan, N. Investigation on the fusion zone microstructures and mechanical integrity of AISI 904L and Inconel 625 weld joints. *Mater. Res. Express* **2019**, *6*, 086540. [CrossRef]
33. Wang, H.; Turner, J.A. The Corrosion of a Stainless Steel in High Temperature Phosphoric Acid. *ECS Trans.* **2019**, *13*, 133–141. [CrossRef]
34. Choudhary, B.K.; Isaac Samuel, E.; Bhanu Sankara Rao, K.; Mannan, S.L. Tensile stress-strain and work hardening behaviour of 316LN austenitic stainless steel. *Mater. Sci. Technol.* **2001**, *17*, 223–231. [CrossRef]
35. Tehovnik, F.; Burja, J.; Arh, B.; Vode, F. Precipitation of σ phase in superaustenitic stainless steel UHB 904L. *Metalurgija* **2017**, *56*, 63–66.
36. Gras, J.M. *Applications of Electricity and Corrosion. Precautions for Use of Metals and Stainless and Refractory Alloys*; EDF: Clamart, France, 1993.

37. Ahlblom, B.; Sandstrom, R. Hot workability of stainless steels: Influence of deformation parameters, microstructural components, and restoration processes. *Int. Met. Rev.* **1982**, *27*, 1–27. [CrossRef]
38. Kim, Y.H.; Lee, D.J.; Byun, J.C.; Jung, K.H.; Kim, J.I.; Lee, H.J.; Shin, Y.T.; Kim, S.H.; Lee, H.W. The effect of sigma phases formation depending on Cr/Ni equivalent ratio in AISI 316L weldments. *Mater. Des.* **2011**, *32*, 330–336. [CrossRef]
39. Lin, Y.C.; Nong, F.Q.; Chen, X.M.; Chen, D.D.; Chen, M.S. Microstructural evolution and constitutive models to predict hot deformation behaviors of a nickel-based superalloy. *Vacuum* **2017**, *137*, 104–114. [CrossRef]
40. Li, N.; Wang, Y.D.; Lin Peng, R.; Sun, X.; Ren, Y.; Wang, L.; Cai, H.N. Synchrotron X-ray diffraction study of texture evolution in 904l stainless steel under dynamic shock compression. *Metall. Mater. Trans. A Phys. Metall. Mater. Sci.* **2011**, *42*, 81–88. [CrossRef]
41. Ma, M.; Ding, H.; Tang, Z.; Zhao, J.; Jiang, Z.; Li, G. Effect of strain rate and temperature on hot workability and flow behaviour of duplex stainless steel. *Ironmak. Steelmak.* **2016**, *43*, 88–96. [CrossRef]
42. Molnár, D.; Engberg, G.; Li, W.; Vitos, L. Deformation properties of austenitic stainless steels with different stacking fault energies. *Mater. Sci. Forum* **2018**, *941 MSF*, 190–197. [CrossRef]
43. Parvathavarthini, N.; Dayal, R.K. Influence of chemical composition, prior deformation and prolonged thermal aging on the sensitization characteristics of austenitic stainless steels. *J. Nucl. Mater.* **2002**, *305*, 209–219. [CrossRef]
44. Tümer, M.; Yılmaz, R. Characterization of microstructure, chemical composition, and toughness of a multipass welded joint of austenitic stainless steel AISI316L. *Int. J. Adv. Manuf. Technol.* **2016**, *87*, 2567–2579. [CrossRef]
45. Stornelli, G.; Montanari, R.; Testani, C.; Pilloni, L.; Napoli, G.; Di Pietro, O.; Di Schino, A. Microstructure refinement effect on EUROFER 97 steel for nuclear fusion application. *Mater. Sci. Forum* **2021**, *1016*, 1392–1397. [CrossRef]
46. Mancini, S.; Langellotto, L.; Di Nunzio, P.E.; Zitelli, C.; Di Schino, A. Defect Reduction and Quality Optimization by Modeling Plastic Deformation and Metallurgical Evolution in Ferritic Stainless Steels. *Metals* **2020**, *10*, 186. [CrossRef]
47. Stornelli, G.; Gaggia, D.; Rallini, M.; Di Schino, A. Heat Treatment Effect on Maraging Steel Manufactured By Laser Powder Bed Fusion Technology: Microstructure and Mechanical Properties. *Acta Metall. Slovaca* **2021**, *27*, 122–126. [CrossRef]
48. Naghizadeh, M.; Mirzadeh, H. Effects of Grain Size on Mechanical Properties and Work-Hardening Behavior of AISI 304 Austenitic Stainless Steel. *Steel Res. Int.* **2019**, *90*, 1900153. [CrossRef]
49. Masumura, T.; Seto, Y.; Tsuchiyama, T.; Kimura, K. Work-hardening mechanism in high-nitrogen austenitic stainless steel. *Mater. Trans.* **2020**, *61*, 678–684. [CrossRef]
50. Mallick, P.; Tewary, N.K.; Ghosh, S.K.; Chattopadhyay, P.P. Effect of cryogenic deformation on microstructure and mechanical properties of 304 austenitic stainless steel. *Mater. Charact.* **2017**, *133*, 77–86. [CrossRef]
51. Belyakov, A.; Sakai, T.; Miura, H.; Kaibyshev, R.; Tsuzaki, K. Continuous recrystallization in austenitic stainless steel after large strain deformation. *Acta Mater.* **2002**, *50*, 1547–1557. [CrossRef]
52. Padilha, A.F.; Plaut, R.L.; Rios, P.R. Annealing of cold-worked austenitic stainless steels. *ISIJ Int.* **2007**, *43*, 135–143. [CrossRef]
53. Shirdel, M.; Mirzadeh, H.; Habibi Parsa, M. Microstructural evolution during normal/abnormal grain growth in austenitic stainless steel. *Metall. Mater. Trans. A Phys. Metall. Mater. Sci.* **2014**, *45*, 5185–5193. [CrossRef]
54. Stornelli, G.; Di Schino, A.; Mancini, S.; Montanari, R.; Testani, C.; Varone, A. Grain Refinement and Improved Mechanical Properties of EUROFER97 by Thermo-Mechanical Treatments. *Appl. Sci.* **2021**, *11*, 10598. [CrossRef]
55. Chowdhury, S.G.; Das, S.; De, P.K. Cold rolling behaviour and textural evolution in AISI 316L austenitic stainless steel. *Acta Mater.* **2005**, *53*, 3951–3959. [CrossRef]
56. Xu, D.; Wan, X.; Yu, J.; Xu, G.; Li, G. Effect of cold deformation on microstructures and mechanical properties of austenitic stainless steel. *Metals* **2018**, *8*, 522. [CrossRef]
57. Tanhaei, S.; Gheisari, K.; Zaree, S.R.A. Effect of cold rolling on the microstructural, magnetic, mechanical, and corrosion properties of AISI 316L austenitic stainless steel. *Int. J. Min. Metal. Mater.* **2018**, *25*, 630–640. [CrossRef]
58. Di Schino, A.; Kenny, J.M.; Abbruzzese, G. Analysis of the recrystallization and grain growth processes in AISI 316 stainless steel. *J. Mater. Sci.* **2002**, *37*, 5291–5298. [CrossRef]
59. Di Schino, A.; Barteri, M.; Kenny, J.M. Development of ultra fine grain structure by martensitic reversion in stainless steel. *J. Mater. Sci. Lett.* **2002**, *21*, 751–753. [CrossRef]
60. Di Schino, A.; Kenny, J.M.; Salvatori, I.; Abbruzzese, G. Modelling primary recrystallization and grain growth in a low nickel austenitic stainless steel. *J. Mater. Sci.* **2001**, *36*, 593–601. [CrossRef]
61. Hanza, S.; Marohnić, T.; Basan, R. Artificial Neural Networks-Based Prediction of Hardness of Low-Alloy Steels Using Specific Jominy Distance. *Metals* **2021**, *11*, 714. [CrossRef]
62. GilaIvan, J.; Erdakov, I.; Bustillo, A.; Pimenov, D.Y. A regression-tree multilayer-perceptron hybrid strategy for the prediction of ore crushing-plate lifetimes. *Jour. Adv. Rese.* **2019**, *18*, 173–184. [CrossRef]
63. Erdakov, I.N.; Tkachev, V.M.; Novokreshchenov, V.V. Increase of wear resistance of steel plates for crushing stations. *J. Frict. Wear.* **2014**, *35*, 514–519. [CrossRef]
64. Choi, J.S.; Yoon, D.Y. The temperature dependence of Abnormal Graing growth and Grain Boundary Faceting in 316L Stainless Steel. *ISIJ Int.* **2001**, *41*, 478–483. [CrossRef]
65. Momenia, A.; Dehghania, K.; Keshmirib, H.; Ebrahimi, G.R. Hot deformation behavior and microstructural evolution of a superaustenitic stainless steel. *Mater. Sci. Eng. A* **2010**, *527*, 1605–1611. [CrossRef]